Cytotoxic and anti-tumor effects of 3,4-*seco*-lupane triterpenoids from the leaves of *Eleutherococcus sessiliflorus* against hepatocellular carcinoma

Haohao Wang[a1], Wenliu Yu[b1], Danfeng Zhang[a1], Yan Zhao[a]*, Chen Chen[a], Hongyan Zhu[a], Enbo Cai[a], Zhaowei Yan[b]*

a. College of Chinese Medicinal Materials, Jilin Agricultural University, Changchun 130118, China

b. Department of Pharmacy, The First Affiliated Hospital of Soochow University, Suzhou 215006, China

* Corresponding Author: Yan Zhao, College of Chinese Medicinal Materials, Jilin Agricultural University, Changchun 130118, Jilin, China. E-Mail address: zhyjlu79@163.com (Y. Zhao); Zhaowei Yan, Department of Pharmacy, The First Affiliated Hospital of Soochow University, Suzhou 215006, Jiangsu, China. E-mail address: yanzwsuzhou@163.com (ZW. Yan)

1. Haohao Wang, Wenliu Yu and Danfeng Zhang contributed equally to this work.

Abstract

A rich of 3,4-*seco*-lupane triterpenoids (3,4-SLT), including chiisanoside (CSS), divaroside (DVS), sessiloside-A1 (SSA), chiisanogenin (CSG), sessiligenin (SSG), were isolated from the ethanol extract of the leaves of *Eleutherococcus sessiliflorus* (LES). The present study was performed to explore the cytotoxic and anti-tumor effects of the isolated five ones, as well as potential molecular mechanisms. The results of a CCK-8 assay demonstrated that these 3,4-SLT can inhibit the growth of HepG2 cells, and SSG showed the most significant cytotoxicity. Hoechst 33258 fluorescence staining and Annexin V-FITC/PI staining indicated that 3,4-SLT in LES can induce HepG2 cell apoptosis effectively. The AutoDock Vina program was used to simulate molecular docking of drugs and targets to discuss possible pharmacological mechanisms. Besides, western blot and qRT-PCR results indicated that SSG can inhibit PI3K/AKT signaling pathway through controlling multi-targets. This study suggested that 3,4-SLT might become a new research hotspot for antineoplastic drugs.

Keywords

Eleutherococcus sessiliflorus; 3,4-*seco*-lupane triterpenoids; Anti-tumor; Molecule docking

Experimental

Materials and reagents

The air-dried leaves of *E. sessiliflorus* was collected from the Changbai Mountain area in China. CSS, DVS, SSA, CSG and SSG were prepared by ourselves; cyclophosphamide (CTX) was purchased from the Affiliated Hospital of Changchun University of Traditional Chinese Medicine (Changchun, China); The human normal liver cell line L02 cell and the hepatocellular carcinoma HepG2 cell line were obtained from Cell Bank of Typical Culture Preservation Committee of Chinese Academy of Sciences (Shanghai, China) (specimen numbers: GNHu 6 and SCSP-510); Fetal bovine serum (FBS), RPMI 1640 medium were purchased from Gibco (Grand Island, NY, USA); Phosphate buffered saline (PBS), penicillin and streptomycin were purchased from Hyclone (Logan, Utah, US); Hoechst 33258 stain was obtained from Solarbio (China); Annexin V-FITC/PI Apoptosis Detection Kit was obtained from BestBio Biotechnology Co., Ltd (China); Cell lysis buffer for qRT-PCR and western blotting were purchased from Bioss Biotechnology Co., Ltd (China); GAPDH, Bax, Bcl-2, p-PI3K and p-AKT monoclonal antibodies were also purchased from Bioss Biotechnology Co., Ltd (China); The purities of CSS, DVS, SSA, CSG and SSG were determined by HPLC, and the structures were identified by NMR. Other reagents and chemicals used in the study were of analytical grade.

Extraction Separation and characterization method of 3,4-SLT from Eleutherococcus sessiliflorus leaves

All samples were harvested from Jilin Province, China, and identified by Professor Yan Zhao (College of Chinese Medicinal Materials, Jilin Agricultural University, Changchun, China). The voucher specimens (No. 20180711-20180830) had been deposited at the College of Chinese Medicinal Materials, Jilin Agricultural University, Changchun, China.

The dried leaves of *Eleutherococcus sessiliflorus* were extracted by sonication with 75% ethanol. And then the filtrate was dried under reduced pressure to obtain the

crude product (260 g). The crude product (20 g) was then added to a 10% NaOH solution (200 ml) and refluxed at 100°C for 6 h. After cooling, the reaction mixture was neutralized with hydrochloric acid solution, then the mixture was filtered and washed with distilled water to obtain the extract (4.2 g). Subsequently, this extract was chromatographed on a silica gel column and eluted with chloroform-methanol (100 : 1 ~ 3 : 1) to successively obtain CSS (13 mg), DVS (4 mg), SSA (6 mg), CSG (28 mg) and SSG (827 mg). HPLC analysis was carried out on a CXTH-3000 series HPLC chromatographic system. The column was Odyssll C_{18} column (200 mm × 4.6 mm, 5 μm), and the column temperature is 40 ℃, with detection wavelength of 205 nm. The mobile phase was a gradient elution with acetonitrile-water (0-10 min, 35 : 65 - 90 : 10; 10 - 15 min, 90 : 10; 15 - 17 min, 90 : 10 - 35 : 65; 17-20 min, 35 : 65) at a constant flow rate of 1.0 mL/min and the sampling amount was 10 μL.

Cell culture

L02 and HepG2 cells were cultured in a humidified atmosphere containing 5% carbon dioxide at 37°C and using RPMI 1640 containing 10% heat-inactivated fetal bovine serum, 1% glutamine, and 1% penicillin-streptomycin. Cells were used for study when they attained approximately 80% confluence.

Cell viability assay

L02 and HepG2 cells were plated in 96-well plates at 1×10^5 cells per well and cultured in an incubator maintained at 37 °C with 5% CO_2 for 24 h. Afterward, the culture medium was removed and the cells were treated with 200 μL culture medium containing drugs at different concentrations. After incubation for 48 h, the culture medium containing 10 % CCK-8 was added and incubated for 3 h. The absorbance value was measured at 450 nm on a microplate reader.

Nuclear staining with Hoechst 33258

L02 and HepG2 cells were plated on 6-well plates at 1×10^5 cells per well and cultured in an incubator maintained at 37 °C with 5 % CO_2 for 48 h. Afterward, HepG2 cells were then fixed with 1 mL 4 % (w/v) paraformaldehyde in PBS for 1 h at 4˚C. And then the cells were washed twice with PBS and stained with Hoechst 33258

at room temperature in the dark for 5 min. The cells were subsequently examined and images were captured under a fluorescence microscope.

Flow cytometer analysis of cellular apoptosis

Cellular apoptosis was evaluated by using an Annexin V-FITC/PI Apoptosis Detection Kit according to the manufacturer's instructions. Briefly, cells in all groups were washed twice with ice-cold PBS and then resuspended in binding buffer. Thereafter, cells were subjected to Annexin V-FITC-propidium iodide (PI) double staining and then analyzed on the flow cytometer (BD Biosciences, CA, USA). Data were analyzed by using the CXP software (BD Biosciences, CA, USA). The number of annexin V-FITC-positive and PI-positive cells in each group was discriminated by counting the cells directly.

Molecular docking

ChemBio3D Ultra 14.0 program was used to construct 3D structures of 3,4-*seco*-lupane triterpenoids, energy minimized, and converted to mol2 files. Afterward, based on previous studies, several proteins or kinase domains related to the tumor were selected and downloaded from the Protein Data Bank (http://www.rcsb.org/), these proteins or kinase domains were JAK (PDB code: 4ZIM), p53 (PDB code: 1Y9H), PI3K (PDB code: 1E7U and 4WWO), p65 (PDB code: 4P90). Proteins were loaded into the PyMol program, a compelling molecular visualization tool used to deliver and animate 3D structures (Lill and Danielson 2011). They were divided into receptor and ligand, and then AutoDock Tools 1.5.4 (ADT) was used to prepare input PDBQT files and to calculate a grid box. AutoDock Vina 1.1.2 was also used to dock and predict the binding affinity (kcal/mol) of 3,4-SLT (Trott and Olson 2010). Theoretical results of the molecular docking were compared with the experimental data in HepG2 cells. Finally, identification of interacting residues at distances lower than 4Å was carried out by using PyMol program, and visualize the binding of drugs and ligands.

Western blotting detection in HepG2 cells

The protein levels of Bax, Bcl-2, p-PI3K, and p-AKT in HepG2 cells after treating with SSG were analyzed by western blotting. Total proteins of HepG2 cells

were extracted, and the BCA Protein Assay was performed, according to the manufacturer's protocol to assay the total protein concentration (Cao et al. 2016). Equal protein extracts were then separated on 12 % sodium dodecyl sulfate-polyacrylamide gel electrophoresis (SDS-PAGE) and transferred to polyvinyl difluoride (PVDF) membranes. After being blocked in 5 % skimmed milk in Tris-buffered saline-0.1 % Tween-20 (TBST) for 2 h at room temperature, they were then incubated at 4 °C overnight with different primary antibodies. Sequentially membranes were washed with TBST and incubated with secondary antibodies for 2 h at room temperature. Finally, enhanced chemiluminescence was used to detect the protein bands (Amersham International plc., Buckinghamshire, U.K.).

RNA extraction and quantitative real-time PCR

Total RNA was isolated from HepG2 cells using Trizol reagent according to the manufacturer's instructions. The cDNA was synthesized from 1.5 μg of total RNA by the transcriptor first-strand cDNA synthesis kit according to the manufacturer's instructions. RT-PCR was performed in a TaqMan fast universal PCR master mix kit (2×), under the Applied Biosystems Step-One Fast Real-Time PCR System, and results were analyzed with the Sequence Detection Software 2.0. The primer sequences were listed as follows: Bax (forward, CGGCGAATTGGAGATGAACT; reverse, CAAACATGTCAGCTGCCACC), Bcl-2 (forward, CCAGCATGCGACCTCTGTTT; reverse, ACTTGTGGCCCAGGTATGCA), Caspase-3 (forward, TCATCCAGTCCCTTTGCAGC; reverse, AGGACTCGAATTCCGTTGCC), Caspase-9 (forward, CCCTGGACTGCTTTGTGGTG; reverse, GGACACGGAGCATCCATCTG), GAPDH (forward, GGCAAATTCAACGGCACAGT; reverse, ACGACATACTCAGCACCGGC). The results are expressed as the ratio of optical density to GAPDH.

Animals

Six weeks old male Kunming mice (20.0 ± 2.0 g) were purchased from the Changchun Yisi experimental animal Technology Co. Ltd. (Changchun, China). The

mice were maintained in cage housing in a specifically designed pathogen-free isolation facility with a 12/12 h light/dark cycle.

Animal care and the general protocols for animal use were approved by the Institutional Animal Care and Use Committee of Jilin Agricultural University.

Mouse H_{22} tumor-bearing model

Mouse hepatoma 22 (H_{22}) cells were obtained from the Cell Bank of Typical Culture Preservation Committee of Chinese Academy of Sciences (Shanghai, China). After 7 days, the injection of H_{22} cells into the abdominal cavity of Kunming mice was carried out; the ascites were taken from the mouse and diluted with physiological saline to 1×10^7 cells per ml. Then, 0.2 mL of the cells were inoculated through subcutaneous injection at the right armpit of a mouse to establish a solid tumor model.

Animal treatment and experimental design

Before carrying out the animal experiment, we measured the bodyweight of each mouse. The H_{22} tumor-bearing mice were randomly divided into 9 groups (n=10). Drug administration began after 24 h and was treated once a day for 14 days. The groups for CSS, DVS, SSA, CSG, and SSG administration were respectively given at identical molar ratio (200 μM/kg) by intragastrical. The positive control group was treated with CTX by intraperitoneal injection (25 mg/kg), while the normal group and the model group mice were received 0.9 % normal saline.

All mice were weighed every day and sacrificed 14 days later. All of the mice of each group were weighed, sacrificed, and then tumors were collected to detect the inhibition rate. The tumor inhibitory rate (TIR) was calculated by the following formula: TIR (%) = (tumor weight of model group - tumor weight of treated group) / tumor weight of model group × 100%.

Statistical analysis

Data are expressed as the mean ± S.D. The statistical significance of the differences between the groups was evaluated by the *t*-test and one-way analyses of variance (ANOVAs), followed by the *post hoc* multiple comparison test. $p < 0.05$ was considered to be significant and $p < 0.01$ highly significant.

Discussion

Hepatocellular carcinoma (HCC) is one of the most common types of tumors in the world, with high rates of incidence and disease-related mortality and morbidity in the world (Chen et al. 2006). Despite that a ton of important advances in the treatment of HCC have obtained during the last decades (Llovet et al. 2015), liver resection remains the main curative treatment for HCC patients worldwide currently. However, prognosis after liver resection was still unsatisfied due to the high postsurgical rates of tumor recurrence and metastases (Bruix et al. 2016). Meanwhile, most of the clinical drugs have serious side effects, such as causing liver and kidney dysfunction and reducing immune function. Hence, it is urgent to explore the molecular mechanism of HCC and develop the new target drugs for HCC. In the present study, we offered several lines of evidence for the significant anti-tumor activity of five major 3,4-SLT, and clarified their possible molecular mechanisms.

As we all know, uncontrolled proliferation is one of the main features of tumors, and inhibition of tumor proliferation is one of the most important indicators for the development of anticancer drugs (Lei et al. 2017; Fan et al. 2017). In this study, human hepatoma HepG2 cells were used as the research object to detect the effects of five main 3,4-SLT in the LES. The results showed that SSG could be the main anti-tumor active ingredient.

Tumor formation is largely due to abnormal apoptosis and the unlimited proliferation of abnormal cells (Peng et al. 2015; Peng et al. 2015). Apoptosis is a process of programmed cell death that leads to morphological, genetic, and intracellular structural changes in the cells (Chawla-Sarkar et al. 2003), which mainly divided into two main ways, one is the extrinsic death receptor-mediated pathway and the other is an intrinsic mitochondria-mediated pathway. In this study, Hoechst 33258 fluorescence staining and Annexin V-FITC/PI staining were used to analyze the apoptosis of HepG2 cells induced by five main 3,4-SLT in the LES. Our results showed that SSG showed the most remarkable apoptosis compared with the control group. This result proved our previous conjecture of that SSG is the main source of anti-tumor activity in the five main 3,4-SLT.

To simulate molecular docking of drugs and targets to discuss possible pharmacological mechanisms, a molecular docking technique has been used. Molecular docking is a computational procedure that attempts to predict the

noncovalent binding of macromolecule (receptor) and a small molecule (ligand) efficiently. According to the experimental data and molecular docking simulation, the potential signaling pathway and the structure-activity relationship of the five main 3,4-SLT in LES were analyzed. The simulation results indicated that PI3K may be a potential target for the influence of the five main 3,4-SLT on tumor cell apoptosis. We found that the activity evaluation of these compounds is gradually enhanced with the removal of the glycosyl group and the 11-hydroxyl and 3-carboxyl formed by the opening of the lactone ring. We hypothesized that the effects of these compounds on tumor cell apoptosis are related to their molecular weights, polarity and the number of hydroxyl and carboxyl groups at the C3 and C11 positions (Feng et al. 2017).

The PI3K/AKT signaling pathway plays a critical role in cell proliferation, survival, and tumor growth (Engelman 2009), activated PI3K can promote cell proliferation and inhibit cell apoptosis. AKT is an important downstream target kinase of the PI3K signaling pathway, activated AKT can inhibit the release of cytochrome c and apoptosis factor, and activate caspase cascade reactions, thereby inhibiting apoptosis and promote the growth of cancer cells. Previous studies showed that Bcl-2 protein family plays a key role in apoptosis (Fulda and Debatin 2006; Philchenkov 2003) Bcl-2 not only can block the release of Ca^{2+} from the endoplasmic reticulum, reduce the activity of Ca^{2+}-dependent endonuclease, thereby blocking apoptosis, but also can prevent activation of caspase and exert its anti-apoptotic effect. Bax is present in the cytoplasm, and it will reach the mitochondrial membrane and form a protein pore when a signal of apoptosis had been received, which promotes the efflux of the corresponding substance into the cytoplasm.

To verifying the results of our molecular docking predictions, SSG, the main source of efficacy in the five main 3,4-SLT, had been selected as a representative for investigating the potential molecular mechanism. Our results showed that SSG resulted in a significant inhibition in constitutively elevated levels of phosphorylated PI3K/AKT significantly in HepG2 cells. AKT can inhibit apoptosis through multiple targets, including Bcl-2 family and caspase proteases. In this study, SSG treatment resulted in a marked decrease of Bcl-2 expression and an increase of Bax expression on the protein level. Meanwhile, the mRNA expression of Bax, caspase-3, and caspase-9 increased and Bcl-2 decreased significantly compared with the control group. Based on these studies, we have reason to believe that SSG induces HepG2 cell apoptosis through multi-targets controlled post-translational regulation of

PI3K/AKT signaling.

As we all know, the effects of anti-tumor in vivo are important indicators to evaluate the effects of drugs. In this study, an H_{22} tumor-bearing mouse model was also established to investigate the anti-tumor activities of the five major 3,4-SLT. The results showed that SSG had the most significant anti-tumor effect. It was worth noting that the lower tumor inhibition rate of SSA might be related to its solubility, which makes it difficult to achieve the effective concentration of SSA in mouse tumors. Besides, the antineoplastic activities of 3,4-SLT in vivo were not consistent with their effects in vitro, which might be related to the metabolism and transformation of drugs in the body (Bae et al. 2001), and we would further explore their pharmacokinetic mechanisms in vivo in subsequent studies.

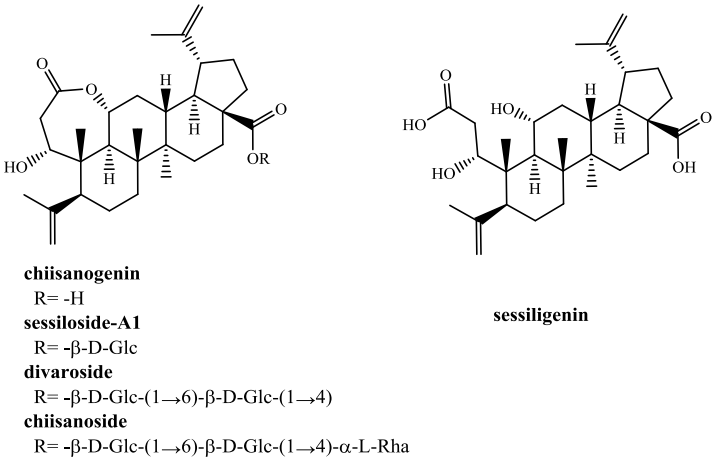

chiisanogenin
R= -H
sessiloside-A1
R= -β-D-Glc
divaroside
R= -β-D-Glc-(1→6)-β-D-Glc-(1→4)
chiisanoside
R= -β-D-Glc-(1→6)-β-D-Glc-(1→4)-α-L-Rha

sessiligenin

Figure S1. Chemical structures of CSS, DVS, SSA, CSG, SSG.

CSS

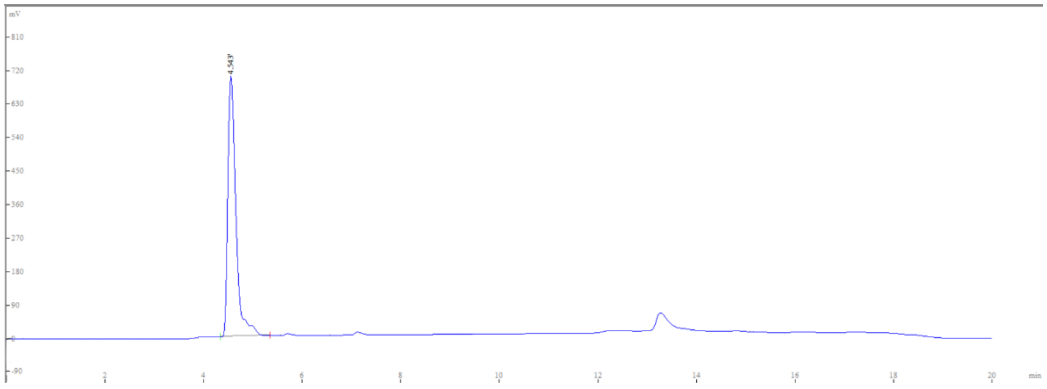

DVS

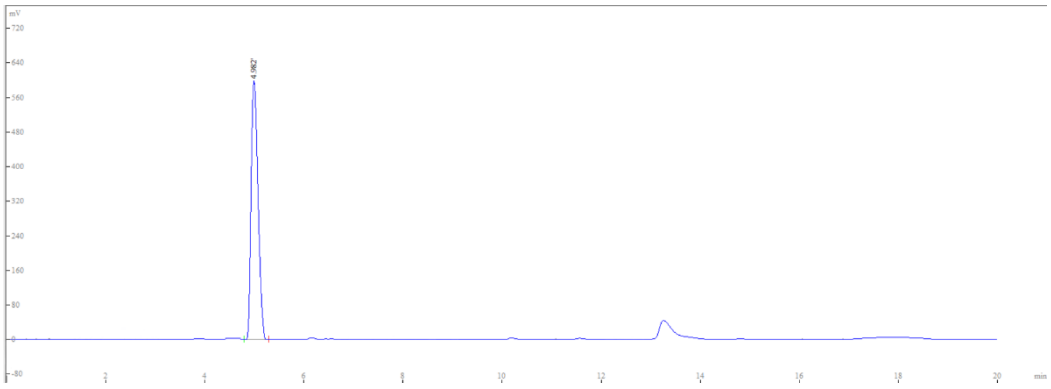

SSA

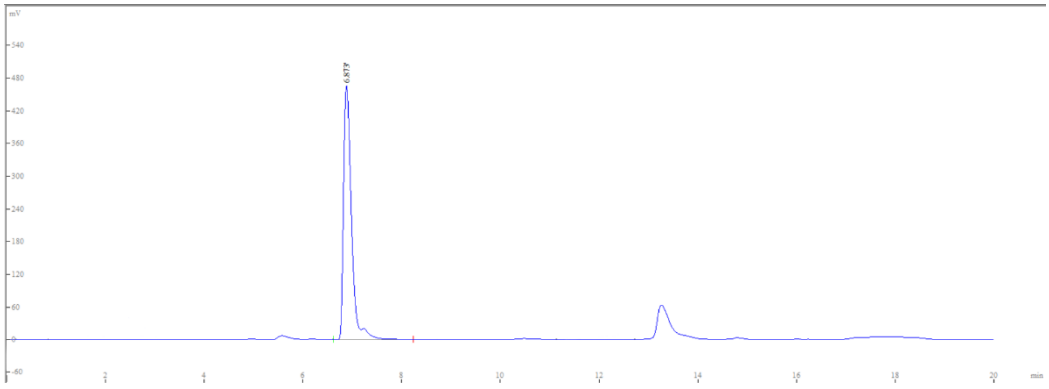

CSG

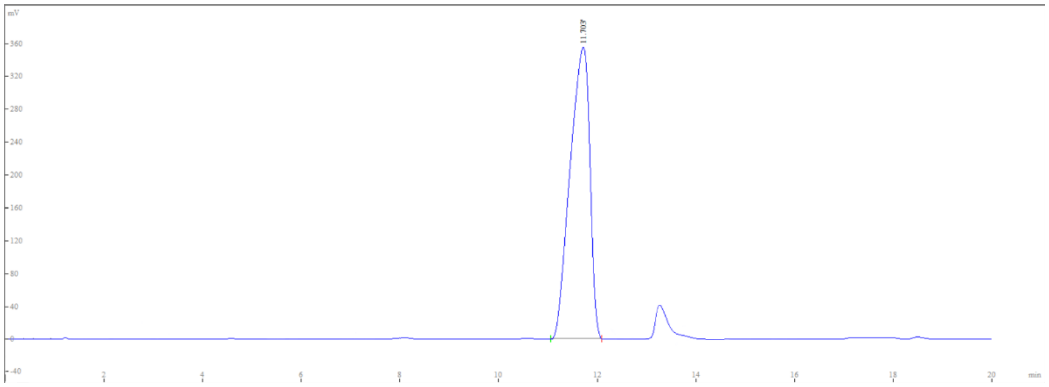

SSG

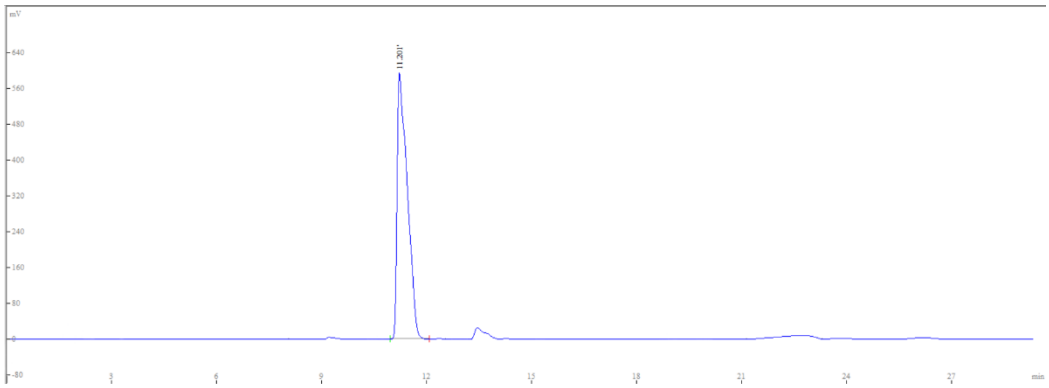

Figure S2. The HPLC chromatogram of 3,4-*seco*-lupane triterpenoids. CSS retention time at 4.543 min; DVS retention time at 4.982 min; SSA retention time at 6.873 min; CSG retention time at 11.703 min; SSG retention time at 11.201 min.

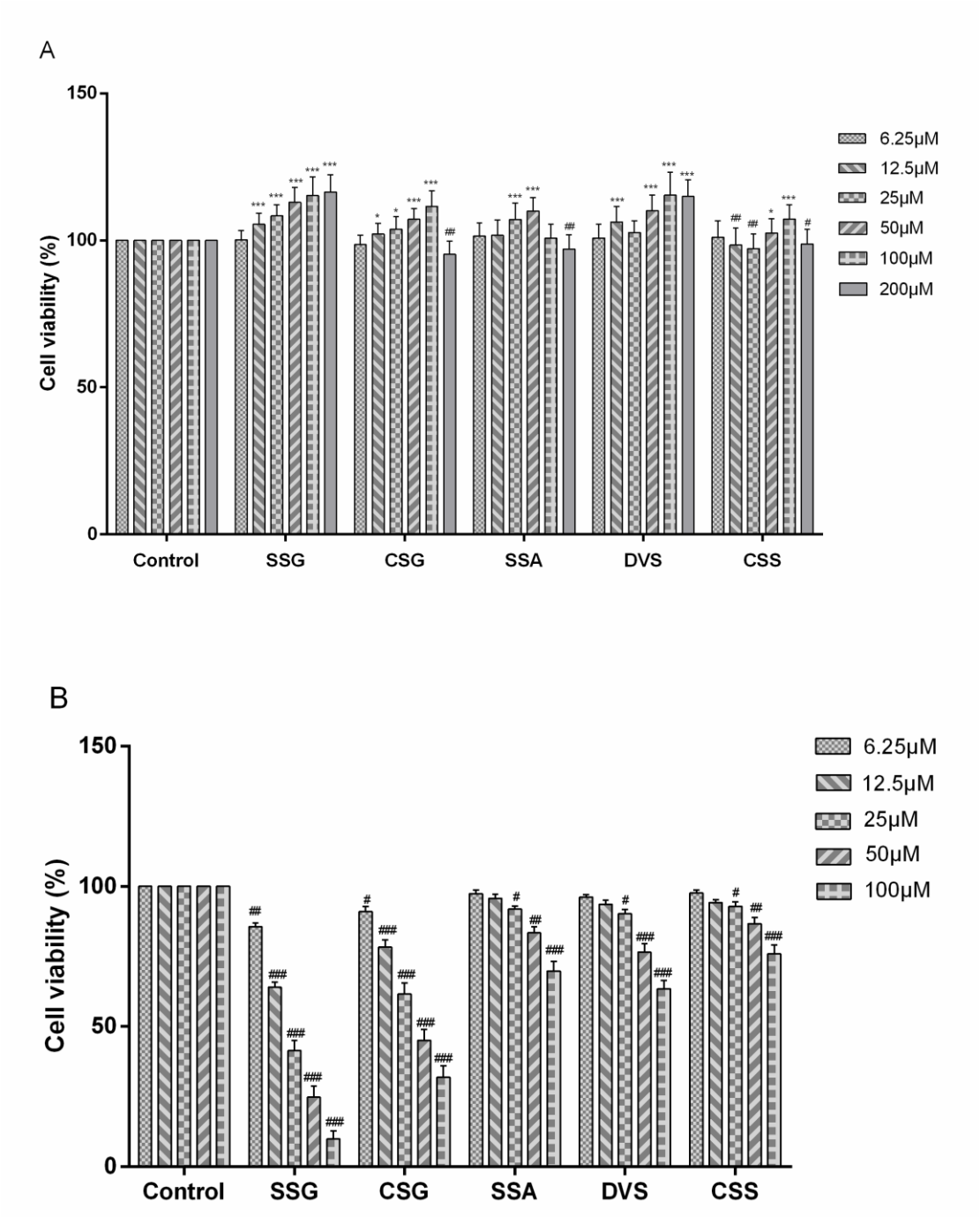

Figure S3. Effects of 3,4-seco-lupane triterpenoids on the viability of L02 (A) and HepG2 (B) cells. Viability of the cells was measured using a CCK-8 assay. Data are expressed as mean ± SD (n = 6). Compared with the control group, when cell viability was increased, * $p<0.05$, ** $p<0.01$, *** $p<0.001$; when cell viability was inhibited, # $p<0.05$, ## $p<0.01$, ### $p<0.001$.

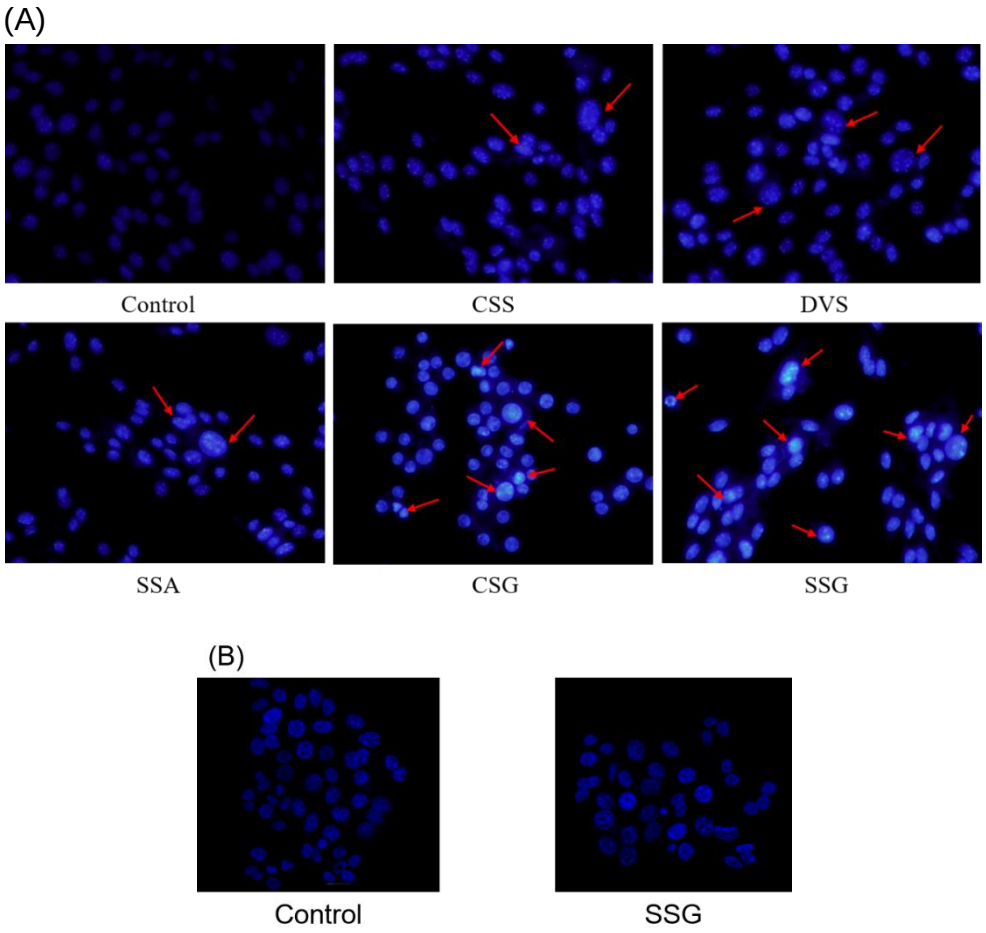

Figure S4. Morphological characterization of L02 and HepG2 cells by fluorescence detection. Cells were stained with Hoechst 33258 and observed by fluorescence microscopy (magnification, ×400). (A) HepG2 cells were treated with 100 μM of CSS, DVS, SSA, CSG and SSG, respectively. Comments: apoptotic cells (red arrow). (B) L02 cells were treated with 100 μM of SSG.

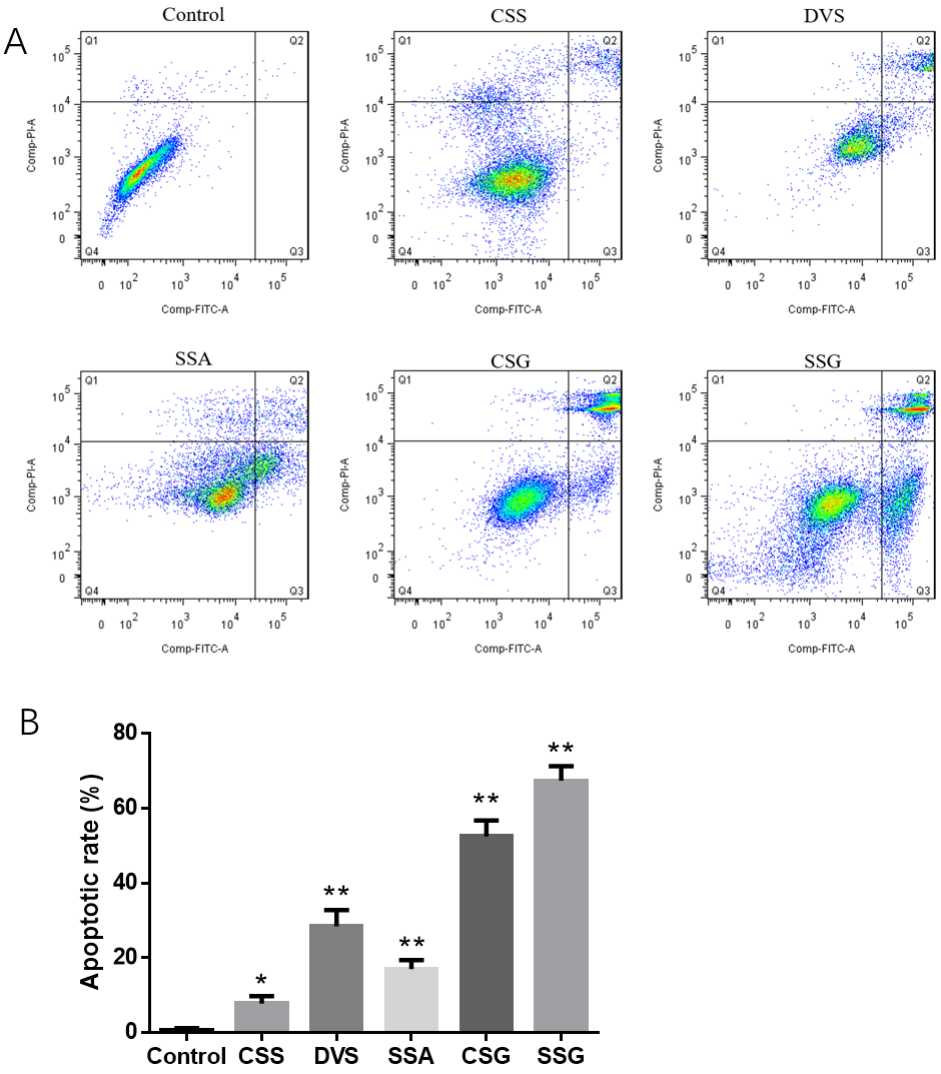

Figure S5. Effects of 3,4-seco-lupane triterpenoids on apoptosis and apoptotic rate in HepG2 cells. (A: HepG2 cells were treated with 100 μM CSS, DVS, SSA, CSG and SSG, respectively; B: apoptotic rate in HepG2 cells) The cell populations of FITC+/PI- and FITC+/PI+ were calculated to represent total apoptotic cells. Data are expressed as means ± SD (n = 6). **p <0.01 vs. control group.

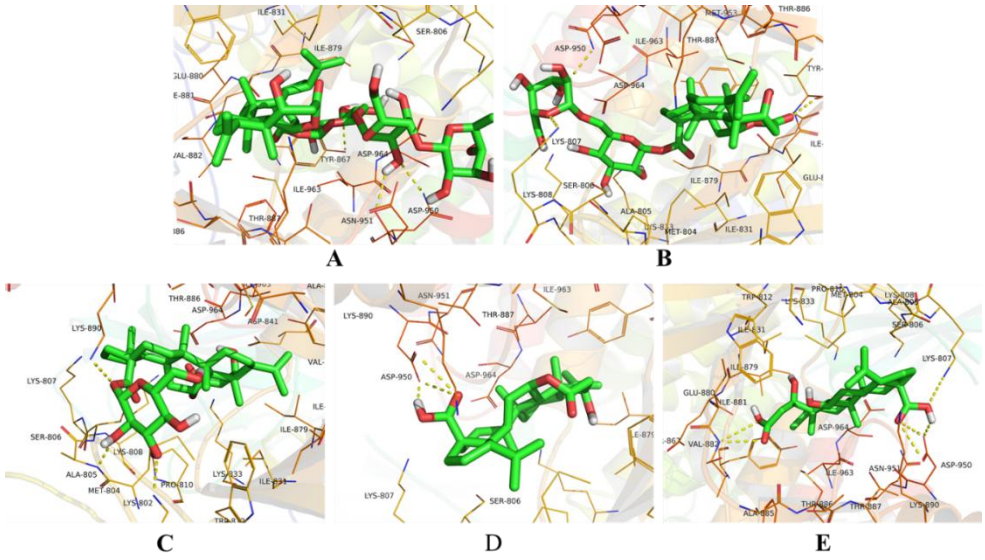

Figure S6. Docking of five 3,4-seco-lupane triterpenoids into the active site of Abl kinase (1E7U) with key amino acid residues in represented ligand binding poses. The pictures were prepared by PyMol software. (A) PI3K - CSS; (B) PI3K - DVS; (C) PI3K - SSA; (D) PI3K - CSG; (E) PI3K - SSG. Comments: H-bonds (yellow dotted line).

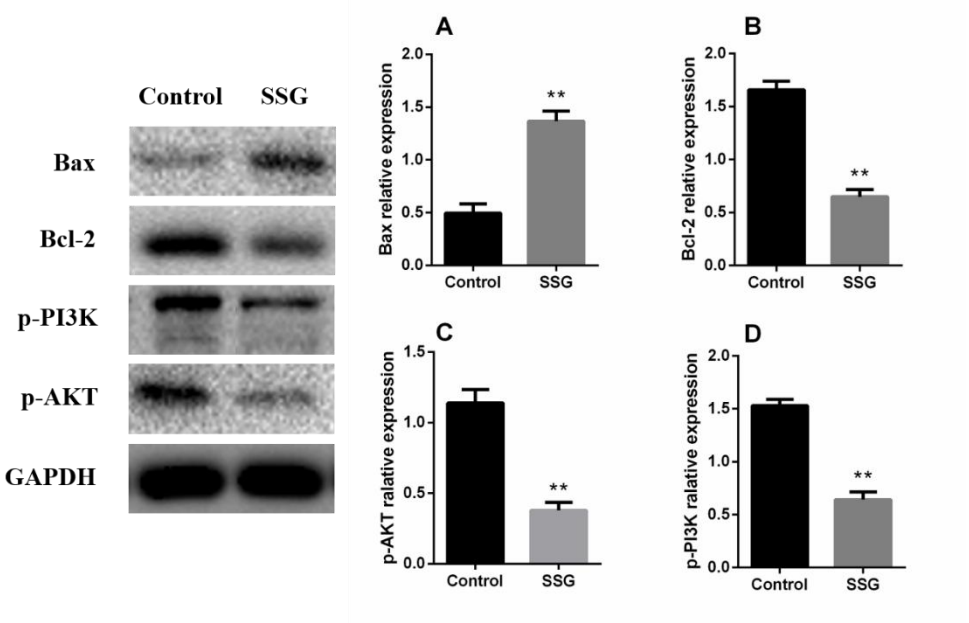

Figure S7. Effects of SSG on protein expression of Bax (A), Bcl-2 (B), p-AKT (C) and p-PI3K (D) in HepG2 cells. GAPDH was used as an internal control. Data are expressed as mean ± SD (n = 3). **p < 0.01 vs. control group.

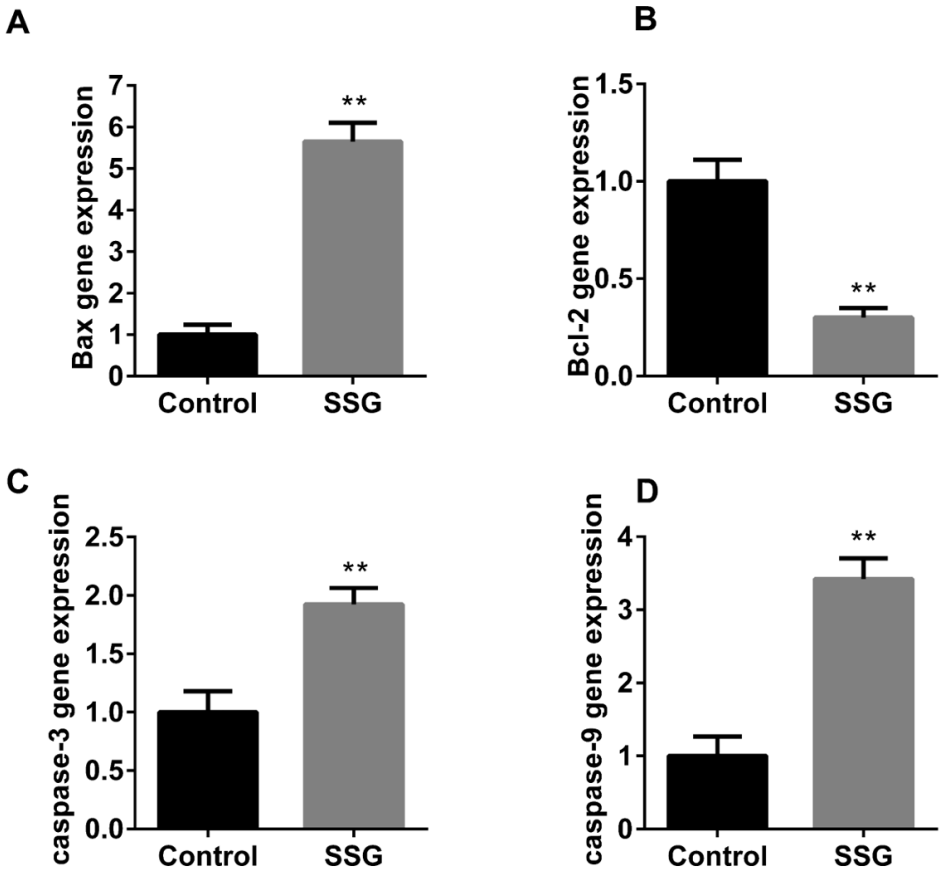

Figure S8. Effects of SSG on gene expression of Bax (A), Bcl-2 (B), caspase-3 (C), caspase-9 (D) in HepG2 cells. GAPDH was used as an internal control. Data are expressed as mean ± SD (n = 3). **p < 0.01 vs. control group.

Table S1. ^{13}CNMR spectroscopic data of 3,4-*seco*-lupane triterpenoids

CSS		DVS		SSA		CSG		SSG	
Position	δ_C: ppm	Position	δ_C: ppm	Position	δ_C: ppm	Position	δ_C: ppm	Position	δ_C: ppm
1	68.74	1	70.63	1	70.54	1	70.69	1	70.82
2	34.30	2	38.03	2	38.83	2	37.10	2	41.96
3	172.75	3	175.56	3	173.05	3	172.62	3	182.02
4	146.83	4	147.53	4	147.75	4	146.35	4	152.82
5	48.76	5	50.09	5	49.62	5	49.67	5	52.72
6	24.56	6	25.35	6	25.22	6	24.16	6	27.53
7	31.12	7	32.64	7	32.39	7	31.50	7	35.17
8	40.87	8	42.20	8	41.78	8	41.08	8	43.75
9	43.17	9	44.26	9	44.15	9	43.34	9	47.63
10	43.39	10	44.17	10	44.12	10	43.42	10	47.87
11	74.26	11	73.41	11	75.30	11	75.20	11	77.97
12	32.61	12	33.56	12	33.53	12	32.08	12	38.33
13	35.89	13	35.61	13	35.27	13	34.67	13	38.69
14	41.46	14	42.40	14	42.23	14	41.47	14	43.93
15	28.63	15	29.63	15	29.58	15	28.79	15	31.16
16	31.65	16	32.11	16	32.17	16	31.64	16	34.78
17	55.92	17	57.12	17	56.81	17	55.70	17	58.94
18	48.48	18	50.20	18	49.78	18	48.74	18	50.58
19	46.65	19	47.76	19	47.65	19	46.63	19	48.28
20	149.65	20	150.46	20	150.16	20	148.53	20	154.97
21	29.98	21	30.87	21	30.82	21	29.98	21	32.32
22	37.94	22	36.73	22	36.73	22	36.35	22	39.08
23	113.52	23	113.65	23	113.93	23	113.71	23	113.22
24	23.62	24	22.60	24	23.56	24	22.08	24	22.83
25	18.44	25	18.70	25	19.05	25	18.53	25	19.80
26	17.29	26	17.52	26	17.91	26	17.47	26	15.95
27	13.37	27	13.37	27	13.83	27	13.37	27	14.83
28	173.92	28	175.59	28	175.00	28	180.14	28	184.47
29	110.47	29	110.23	29	110.76	29	110.52	29	109.70
30	18.77	30	18.51	30	18.95	30	18.46	30	18.20
Glc-1	93.81	Glc-1	94.752	Glc-1	95.55				
Glc-2	72.50	Glc-2	71.141	Glc-2	74.36				
Glc-3	77.00	Glc-3	77.726	Glc-3	79.56				
Glc-4	70.04	Glc-4	71.091	Glc-4	71.11				
Glc-5	76.60	Glc-5	77.236	Glc-5	78.95				
Glc-6	68.08	Glc-6	69.186	Glc-6	62.20				
Glc-1′	102.94	Glc-1′	104.142						
Glc-2′	75.31	Glc-2′	74.506						
Glc-3′	75.62	Glc-3′	76.975						
Glc-4′	77.00	Glc-4′	77.439						
Glc-5′	76.72	Glc-5′	77.275						

Glc-6′	60.18	Glc-6′	62.239
Rha-1	100.63		
Rha-2	70.74		
Rha-3	72.02		
Rha-4	73.84		
Rha-5	69.58		
Rha-6	17.79		

Table S2. Binding Energy predicted by Autodock Vina

Compound	Binding Energy (kcal/mol)				
	4ZIM	1Y9H	1E7U	4WWO	4P90
Original ligand	-10.4	-9.1	-8.1	-10.2	-8.6
CSS	2.6	5.3	-5.3	-3.8	2.3
DVS	-2.2	4.2	-6.3	-4.3	-2.1
SSA	-2.4	-0.6	-7.6	-6.3	-3.2
CSG	-2.8	-0.7	-7.9	-6.7	-3.8
SSG	-3.3	-2.6	-8.0	-7.4	-4.1

Table S3. Effects of five 3,4-seco-lupane triterpenoids on body weight and tumor growth in H_{22} tumor-bearing mice

Groups	Dose	Bodyweight (g)		Tumor weight (g)	TIR (%)
		Pre-treatment	Post-treatment		
Control	Saline	21.42 ± 1.61	27.96 ± 1.33	—	—
Model	Saline	21.21 ± 1.21	30.83 ± 2.28	1.22 ± 0.26	—
CTX	25 mg/kg	22.15 ± 1.34	23.91 ± 1.42	0.45 ± 0.09$^{\#\#}$	63.11
SSG	200 μM	21.82 ± 0.94	27.62 ± 0.84**	0.35 ± 0.08$^{\#\#}$	71.31
CSG	200 μM	21.86 ± 0.82	27.83 ± 0.82**	0.39 ± 0.15$^{\#\#}$	68.03
CSS	200 μM	22.06 ± 1.55	28.58 ± 1.48**	0.44 ± 0.11$^{\#\#}$	63.93
DVS	200 μM	21.74 ± 1.39	28.25 ± 1.29**	0.42 ± 0.16$^{\#\#}$	65.57
SSA	200 μM	22.01 ± 0.56	29.31 ± 0.73**	0.75 ± 0.12$^{\#}$	38.52

Data are expressed as mean ± SD (n = 10), *p < 0.05, **p < 0.01 vs. CTX group, #p < 0.05, ##p < 0.01 vs. model group.

References

Bae EA, Yook CS, Oh OJ, Chang SY, Nohara T, Kim DH. 2001. Metabolism of chiisanoside from Acanthopanax divaricatus var. albeofructus by human intestinal bacteria and its relation to some biological activities. Biol Pharm Bull. 24(5):582-585.

Bruix J, Reig M, Sherman M. 2016. Evidence-Based Diagnosis, Staging, and Treatment of Patients With Hepatocellular Carcinoma. Gastroenterology. 150(4):835-853.

Cao W, Hu C, Wu L, Xu L, Jiang W. 2016. Rosmarinic acid inhibits inflammation and angiogenesis of hepatocellular carcinoma by suppression of NF-kappaB signaling in H22 tumor-bearing mice. J Pharmacol Sci. 132(2):131-137.

Chawla-Sarkar M, Bauer JA, Lupica JA, Morrison BH, Tang Z, Oates RK. 2003. Suppression of NF-kappa B survival signaling by nitrosylcobalamin sensitizes neoplasms to the anti-tumor effects of Apo2L/TRAIL. J Biol Chem. 278(41):39461-39469.

Chen G, Lin W, Shen F, Iloeje UH, London WT, Evans AA. 2006. Past HBV viral load as predictor of mortality and morbidity from HCC and chronic liver disease in a prospective study. Am J Gastroenterol. 101(8):1797-803.

Engelman JA. 2009. Targeting PI3K signalling in cancer: opportunities, challenges and limitations. Nat Rev Cancer. 9(8):550-562.

Fan S, Zhang J, Nie W, Zhou W, Jin L, Chen X. 2017. Antitumor effects of polysaccharide from Sargassum fusiforme against human hepatocellular carcinoma HepG2 cells. Food Chem Toxicol. 102:53-62.

Feng R, Liu J, Wang Z, Zhang J, Cates C, Rousselle T, Meng Q, Li J. 2017. The structure-activity relationship of ginsenosides on hypoxia-reoxygenation induced apoptosis of cardiomyocytes. Biochem Biophys Res Commun. 494(3-4):556-568.

Fulda S, Debatin KM. 2006. Extrinsic versus intrinsic apoptosis pathways in anticancer chemotherapy. Oncogene. 25(34):4798-4811.

Lei YU, Wang X, Chen ZF, Jiang BO, Shang DY. 2017. Cytisine induces apoptosis of HepG2 cells. Mol Med Rep. 16(3):3363-3370.

Lill MA, Danielson ML. 2011. Computer-aided drug design platform using PyMOL. J Comput Aided Mol Des. 25(1):13-19.

Llovet JM, Villanueva A, Lachenmayer A, Finn R S. 2015. Advances in targeted therapies for hepatocellular carcinoma in the genomic era. Nat Rev Clin Oncol. 12(8): 436.

Peng X, Zhang YY, Wang J, Ji Q. 2015. Ethylacetate extract from Tetrastigma hemsleyanum induces apoptosis via the mitochondrial caspase-dependent intrinsic pathway in HepG2 cells. Tumour Biol. 37(1):865-876.

Peng X, Zhuang DD, Guo QS. 2015. Induction of S phase arrest and apoptosis by ethyl acetate extract from Tetrastigma hemsleyanum in human hepatoma HepG2 cells. Tumour Biol. 36(4):2541-2550.

Philchenkov AA. 2003. Caspases as regulators of apoptosis and other cell functions. Biochemistry

(Mosc). 68(4):365-376.

Trott O, Olson AJ. 2010. AutoDock Vina: improving the speed and accuracy of docking with a new scoring function, efficient optimization, and multithreading. J Comput Chem. 31:455-461.